

# MIRGE: An Array-Based Computational Framework for Scientific Computing

MATTHIAS DIENER, MATTHEW J. SMITH, MICHAEL T. CAMPBELL, KAUSHIK KULKARNI, MICHAEL J. ANDERSON, ANDREAS KLÖCKNER, WILLIAM GROPP, JONATHAN B. FREUND, and LUKE N. OLSON\*, University of Illinois Urbana–Champaign, USA

MIRGE is a computational approach for scientific computing based on *NumPy*-like array computation, but using lazy evaluation to recast computation as data-flow graphs, where nodes represent immutable, multi-dimensional arrays. Evaluation of an array expression is deferred until its value is needed, at which point a pipeline is invoked that transforms high-level array expressions into lower-level intermediate representations (IR) and finally into executable code, through a multi-stage process. Domain-specific transformations, such as metadata-driven optimizations, GPU-parallelization strategies, and loop fusion techniques, improve performance and memory efficiency.

MIRGE employs “array contexts” to abstract the interface between array expressions and heterogeneous execution environments (for example, lazy evaluation via OpenCL, or eager evaluation via *NumPy* or *CuPy*). The framework thus enables performance portability as well as separation of concerns between application logic, low-level implementation, and optimizations. By enabling scientific expressivity while facilitating performance tuning, MIRGE offers a robust, extensible platform for both computational research and scientific application development.

This paper provides an overview of MIRGE. We further describe an application of MIRGE called *MIRGE-Com*, for supersonic combusting flows in a discontinuous Galerkin finite-element setting. We demonstrate its capabilities as a solver and highlight its performance characteristics on large-scale GPU hardware.

CCS Concepts: • **Mathematics of computing** → **Mathematical software performance**; • **Computing methodologies** → **Massively parallel and high-performance simulations**; • **Software and its engineering** → **Compilers**.

Additional Key Words and Phrases: array-based, GPU, parallel, numerical PDEs, simulation

## 1 Introduction

The design of scientific simulation software often involves making uncomfortable trade-offs between high-level mathematical abstractions that facilitate understandability and low-level implementation details for performance. The latter can lead to complex codes that make maintenance and portability difficult. In this paper, we present MIRGE (**M**ath–**I**ntermediate **R**epresentation–**G**eneration–**E**xecution), an approach that leverages the high-level usability of Python and targets performance portability across modern and anticipated accelerator architectures.

At the core of MIRGE is a philosophy of *separation of concerns*: the scientific application is written using intuitive array expressions equivalent to *NumPy* expressions in Python, while transformations and optimizations are used to achieve performance. Crucially, these transformations are application-specific (though with reusable parts) and driven by the user through array context customization. This design enables rapid simulation development without precluding the use of performance techniques such as GPU parallelization and loop fusion.

Scientific codes are challenging due to the range of demands, including (1) readability for both domain experts and developers, (2) the need to attain (and maintain) performance on modern

\*Corresponding author.

platforms, (3) ease of maintenance and extension, and (4) identifying performance opportunities and challenges via modeling. One tenet of our strategy is that the clarity of physical and model expressions should not be compromised by implementation details, hardware-specific considerations, or performance optimizations.

MIRGE is an approach that forms the backbone for the implementation of the *MIRGE-Com* simulation library, a solver for high-speed combustion. This approach allows a straightforward description of a computational model that closely resembles the mathematics of the physical model without prescribing platform-specific algorithms that will be used to achieve performance.

In a way, MIRGE takes a similar approach to *JAX* [15] and *torch.fx* [54]. *JAX*, for example, uses what it calls *tracing* to record the operations of a function. It then reconstructs a potentially more efficient function call for execution on devices<sup>1</sup>. *torch.fx* has a focus on capturing *PyTorch* code and transformations for device execution, but has a clear focus “on the DAG representation of deep learning programs.” Similar *graph mode* execution is pursued by a number of codes; MIRGE has a focus on array computations, and consequently PDE-focused numerical simulation. One reason for this is provided by Figure 1. On the left is an example triangular mesh (other meshes may also be used, such as 3D tetrahedral, or quadrilateral and hexahedral meshes which may provide benefits when using a tensor-product basis). In a nodal discontinuous Galerkin setting [31], degrees of freedom (DOFs) are local to an element (as viewed in the middle figure), which has a natural representation in an array format (right figure). As a result, the numerical methods generally operate on arrays of data in bulk, providing an avenue to organize the computation for overall efficiency.

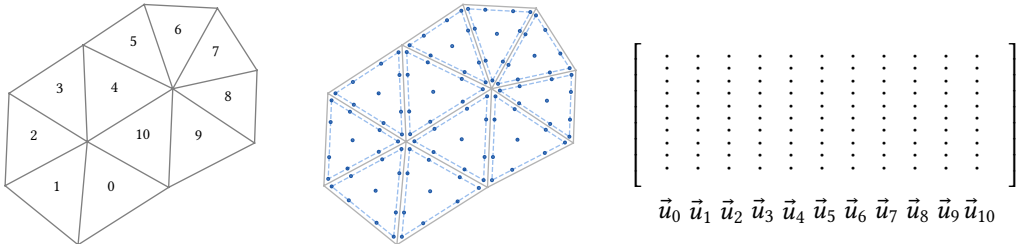


Fig. 1. Discontinuous Galerkin layout. A mesh (left) with nodal degrees-of-freedom local to each mesh element (middle), leads to an array-based layout of the unknowns (right).

MIRGE is one of many approaches to providing user-level productivity (in Python) while pursuing computational efficiency under the hood. *CuPy*, for example, is Python-based with a focus on easily executing *NumPy*-like code on the GPU, providing both drop-in *NumPy* replacements as well as an interface to write kernels directly. Likewise, *PyOpenCL* and *PyCUDA* [38] offer direct access to GPU execution from Python, but offer less drop-in functionality. In this respect, MIRGE has more in common with *CuPy*, but it differs in its focus on providing access to intermediate representations (in part provided by the *loopy* [37] package) in order to facilitate code transformations. Similar transformation-enabling approaches have been developed, for example in *Hercules* [8], which focuses on transformations into parallel code. Their approach concentrates on the IR and transformations, but purposely steps away from existing high-level programming languages such as Python. In contrast, MIRGE strives to make such optimization work more accessible by realizing it

<sup>1</sup><https://docs.jax.dev/en/latest/jit-compilation.html>

as a transformation step within a Python-based processing chain. A further point of differentiation is that the design of MIRGE is not tied to a particular execution target (AMD, NVIDIA, CPUs, etc.); different backends may be used, enabling execution on a variety of platforms.

In the next section, we take an in-depth look at past and present work, broadly categorizing existing approaches and giving a sense of how MIRGE fits among them. Subsequent sections provide an overview of MIRGE, detailing the lazy/JAX-style evaluation for general array-based computation, achieving the overarching goal of benefiting from Python-level semantics with low-level performance. A high-level description of MIRGE is given in Section 3, setting the foundation and providing additional motivations. The details of MIRGE are given in Section 4, where we delve into the intricacies of tracing the array-based code, generating intermediate representations for further optimizations, and ultimately generating code for execution on a variety of platforms. In Section 5, *MIRGE-Com* is introduced, an application of MIRGE for supersonic combusting flows. We provide performance measurements on baseline applications, show comparisons with existing codes, and demonstrate the use of *MIRGE-Com* in practice.

## 2 Related Work

Array programming as a paradigm has been studied extensively. Early systems such as *Fortran-I* [10] introduced multidimensional arrays primarily as a storage format. Iverson et al. [23] designed *APL*, which adopted notation from tensor analysis to represent  $n$ -dimensional arrays. Every object in *APL* is an array, and the language supports high-level routines such as reshaping, rank querying, and inner or outer-products. Successors to *APL* include *J*, *K*, *MATLAB*, *NumPy* [30], and *Julia* [14], all of which have contributed to the popularization of array-centric computing for a wide range of scientific applications.

Two key factors influence the usability of an array programming system for computational science workloads. The first is its *execution throughput*, which determines the scale of problems that can be solved within a given amount of compute time. The second is the *debuggability* of the system, which governs the speed at which computational scientists can program their workloads. Improved debuggability enables inspection of intermediate program states, thereby accelerating the development process. Both characteristics are direct consequences of the system's execution model.

Toolkits like *NumPy*, early versions of *Torch* [51], *CuPy* [50], *APL*, and *ArrayFire* [46] employ an *eager evaluation* model. In this model, each operation is executed as soon as it is encountered, with its result persisted in memory. This allows progressive evaluation [28] of the program which aids in rapid prototyping, but incurs performance overheads due to frequent memory roundtrips for the operands and, in a GPU setting, repeated kernel launches. An alternative is the *deferred evaluation* programming model, where a computational graph is constructed from the program, which is subsequently lowered by a compiler and executed through a runtime layer. These frameworks address much of the previously covered performance limitations, by techniques such as kernel fusion, and, using tuned micro-kernel libraries such as *BLAS* [17], *cuDNN* [20]. Examples of such systems include, *Tensorflow* [1], *JAX* [25], *Julia* [14], *Torch.fx* [54], *Theano* [57], and *Legate* [13]. The runtime layers construct an IR corresponding to the user's program either via tracing [25], or abstract syntax tree (AST) traversal [43] or a combination of both [58]. The IR corresponding to the user's program is subsequently leveraged by optimizing compilers.

By design, deferred evaluation is amenable to more sophisticated optimizations than eager evaluation because the compiler has additional information about the users of intermediate array operations. This information is crucial for many compiler techniques, including kernel fusion [39], array contraction [26], and data-layout transformations. Transforming an array graph into a computational kernel that achieves near-roofline performance is challenging primarily because of the

large transformation space, which includes the selection of execution-grid sizes, decisions about materialization, the choice of address spaces, and more. Prior work has shown that many subproblems within the lowering process are NP-hard. For example, Rosenkrantz et al. [56] established that deciding which arrays to materialize is NP-complete; Lam et al. [42] demonstrated that choosing the optimal contraction path for Einstein summations is NP-hard; and Kennedy et al. [35] showed that loop fusion for maximizing data reuse is also NP-hard. Consequently, many array frameworks adopt a pragmatic choice by restricting the scope of compiler optimizations to those applicable to a particular domain. This trend is evident in frameworks such as *TensorFlow*, *Jax*, and, *torch.fx*, which are primarily used in machine-learning applications since the profitability of their embedded compiler optimizations does not transfer to other domains.

Multidimensional arrays are a fundamental data-structure widely seen across various fields of scientific computing. However, we are not aware of any state-of-the-art simulation engine that natively uses any of the array frameworks mentioned above. Representative examples include *Nek5000* [49, 24], which is a *Fortran*-based Finite Element Methods (FEM) solver that provides FEM-specific high-level routines for defining the weak-form. Abdelfattah et al. [2] further optimized it for high-performance architectures. *MFEM* [7] is a C++ FEM library that integrates optimized assembly kernels from *libCEED* [16] and leverages iterative solvers from *PETSc* [11]. The Unified Form Language (UFL) [3] provides a high-level abstraction for weak formulations in the Ciarlet framework [21], serving as the frontend for end-to-end solvers such as *FEniCS* [4], *Firedrake* [53], and *Dune* [12]. These systems compile user-defined variational forms into efficient kernels through FEM-specific optimizations [36, 33, 41].

Despite these advances, integrating user-defined array expressions into such solvers remains impractical due to significantly low performance relative to the roofline. Prior efforts have partially addressed these concerns. Hirata [32] proposed *Tensor Contraction Engine*, which provided high-level operations for electronic structure computations, and allowed for user-specified computations that were a subset of the tensor contraction operations using the einsum notation. Similarly, *Comet* [48] allows computational chemistry programs to be expressed in a subset of *NumPy*, lowering computations through the tensor algebra dialect of *MLIR* [44] and applying optimizations such as Transpose-transpose-GEMM-transpose [32].

In this work, we present a framework for scientific simulation development, together with an application to a discontinuous Galerkin (DG) FEM solver, in which arrays are the sole user-facing data-type. Users can express computations entirely through high-level array operations encompassing a pure subset of *NumPy*, i.e., a set of operations that disallows in-place modification. We lower the resulting array graph through our *Pytato/Loopy* IR to address a key limitation observed in prior work: the inability to inject domain-specific code transformations.

### 3 The MIRGE Approach

Figure 2 illustrates the MIRGE approach, from domain-specific math (left) to transformed, host-specific computational kernels (middle) to code generation and execution on target platforms (GPUs or CPUs). The non-optimized eager path, shown as a dashed grey line (top), is a fall-back approach outside the intended *lazy* processing path for execution. This approach is novel in predictive science and provides a two-way street between performance research and scientific simulation by allowing access to large-scale predictive science applications and by delivering the performance benefits directly to the application.

We make use of a pipeline that uses lazy execution to enable code transformations. This relies on a user-facing layer of *NumPy*-like array constructs (an *array context*) that internally captures computation symbolically, deferring execution to enable performance optimizations and to target different execution environments, such as GPUs. Arrays in this framework are considered immutable

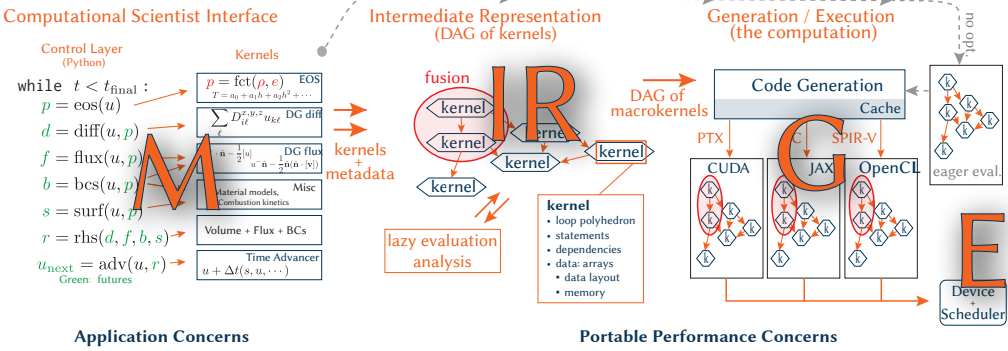


Fig. 2. The MIRGE approach to scientific computing. (Left) the domain-specific math, (middle) the optimized, host-specific computation kernels, and (right) generation and execution of platform specific code.

objects that represent the fundamental building blocks of the computation. By evaluating the program in this manner and producing an *array dataflow graph* (ADFG), a comprehensive view of the user’s intended computation is available and transformations such as fusion and parallelization can be applied. An example of the user-facing part of this is shown on the left side of Figure 3. Here, array operations in `axy_max0()` are evaluated symbolically and code is generated from the resulting ADFG, which is then executed.

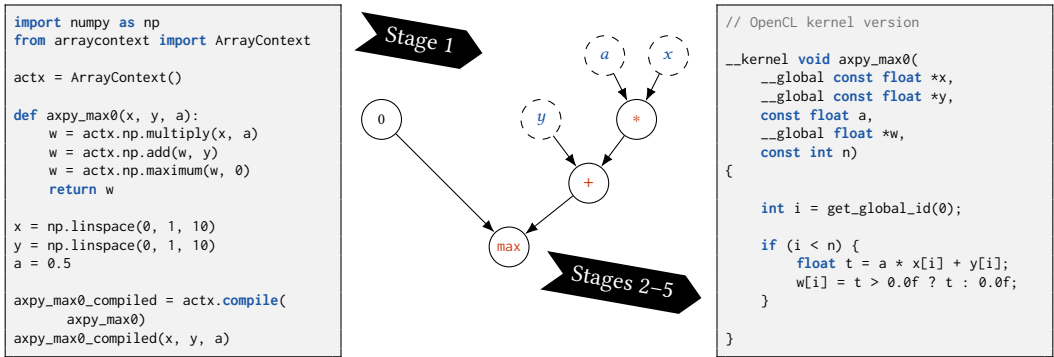


Fig. 3. Stages 1 and 2–5 of the MIRGE approach for an example operation on two arrays  $x$  and  $y$  (with scalar  $a$ ):  $\max(0, y + ax)$ . (Left) *NumPy*-like application code using the MIRGE approach. (Middle) The array dataflow graph (ADFG), with the nodes representing array-valued expressions, while the edges represent dependencies between them. (Right) Generated OpenCL code after the transformations in the previous.

How does the simulation unfold? Over several stages the steps of the computation are collected, transformed into a target language (e.g. OpenCL), and executed:

**Stage 1: Capture an Array Dataflow Graph (ADFG)** The pipeline begins by representing the mathematical steps of computation as an array dataflow graph (ADFG), where each node represents an array or array operation. The calculation, represented as a *NumPy*-like array program, is traced symbolically to assemble the ADFG. Tracing proceeds until the execution reaches a user-defined stopping point (via `actx.freeze()`/`actx.compile()`), at which

point the rest of the code generation pipeline is triggered. Figure 3 shows the ADFG in the middle; nodes represent array-valued expressions, while the edges represent dependencies between them.

- Stage 2: Transform the ADFG** Next, domain-specific transformations are applied to the ADFG, such as algebraic simplifications and an initial decision on materialization, that is, whether any given intermediate value is stored in memory. Much of this process is driven by sparse, descriptive metadata that is attached to the ADFG nodes in Stage 1 by user or library code.
- Stage 3: Rewrite to a Scalar Intermediate Representation (IR)** Next, the transformed ADFG is converted into a scalar (loop-level) intermediate representation (IR), which introduces loop structures and memory allocations. Metadata may also propagate into the IR in the next stage, as metadata on loop variables, for example. While the ADFG expresses *what* should be computed, the IR expresses *how* it should be computed, including execution order and memory ordering.
- Stage 4: Transform the Scalar IR** With this IR, transformations for parallelization and memory access are applied. For example, it is often advantageous for loops to be partitioned into block/thread structures. Additionally, metadata, propagated from prior stages, may be used to determine which loops to fuse and how to map array axes onto parallel hardware. This stage is home to much of the performance-tuning work, and is an opportunity to link with external tools.
- Stage 5: Emit Generated Target Code** After optimization transformations, the IR is used to generate target code. Our examples use OpenCL, though JAX or CUDA are other options. This stage also translates higher-level constructs into efficient low-level code, potentially relying on OpenCL-specific code for memory access and parallel execution.
- Stage 6: Program Execution** In the final stage, the compiled kernel is executed on the target hardware. The array context manages the memory allocation, the OpenCL execution context, and the launching of kernels. Since earlier stages have already optimized and compiled the program, the runtime overhead is minimal.

We make use of two separate intermediate representations in our transform chain to focus on distinct aspects: The ADFG for the most part does not represent ‘space’ (memory) and ‘time’ (evaluation order and parallelization), and thus transformations applied at its level are mostly of an algebraic nature. Meanwhile, optimizations that depend on these specifics are applied at the level of the scalar/loop-level IR.

#### 4 Stages of a Computation: Finer Points

The previous section provided a high-level overview of the overall approach to MIRGE. Next, we examine the details, highlighting necessary pieces for generality and for achieving performance at scale.

As previously mentioned, array operations in MIRGE are expressed using NumPy-like *array contexts*. Nominally, array contexts control the execution of the array programs supplied by the user. More specifically, this involves choice of the execution environment and control of program transformation for high performance. To this end, the array programming interface provided is focused on facilitating lazy evaluation, though other execution environments are also available, cf. Table 1.

To give the reader a sense of the complexity of processing applied at the various stages of the transform chain, Figure 4 shows a breakdown of the fraction of time spent at each stage for an example problem (a compressible multispecies flow case similar to the case presented in Section 5.4, with a smaller mesh of approximately 200K degrees of freedom). In our applications, the processing

Table 1. Overview of eager and lazy evaluation array contexts. The **Lazy PyOpenCL-based** array context is described in detail in this paper.

Eager evaluation array contexts	Lazy evaluation array contexts
Eager PyOpenCL-based	<b>Lazy PyOpenCL-based</b>
<i>JAX-eager</i>	<i>JAX-lazy</i>
<i>NumPy</i>	
<i>CuPy</i>	

time has little to no dependence on the sizes of the array data. There is some dependence on the layout of data across processors in distributed environments, but this is bounded: it grows with the number of adjacent neighbor processors, which eventually saturates. Instead, scaling has a complex dependence on the amount and nature of the work specified in the application code. Stages 1 and 2 generally scale with the number of nodes in the ADFG, whereas the latter stages introduce additional scaling dependencies, such as the number of generated statements and the relationships between them. In practice, the illustrated chart is qualitatively representative of what we observe for most problems. Thus, our primary approach to managing processing time has been to employ strategies to minimize the size of the initial ADFG (see Section 4.1.3 for an example).

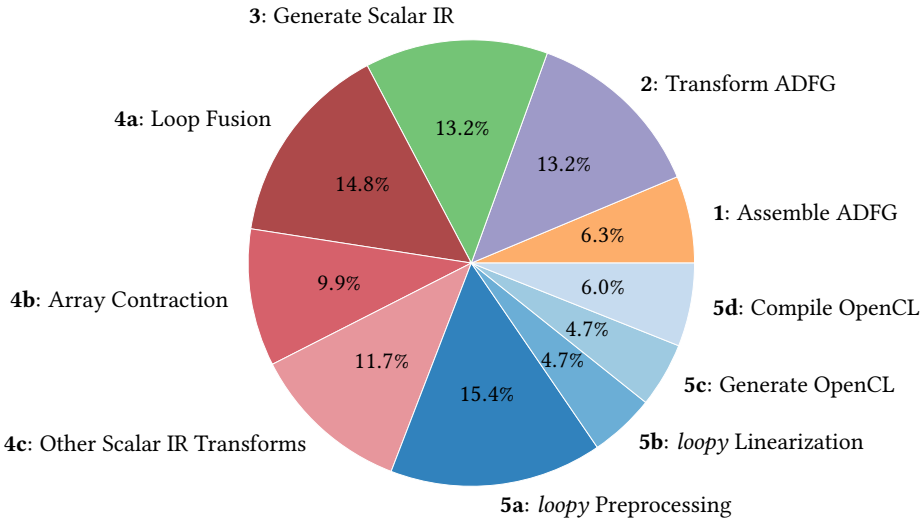


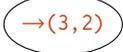
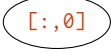
Fig. 4. Breakdown of time spent in pre-execution stages for an example case.

#### 4.1 Stage 1: Capture an Array Dataflow Graph (ADFG)

The first stage of the compilation pipeline begins by capturing a symbolic representation of the computation, i.e., the ADFG. Various node types are used to represent the operations; Table 2 summarizes some of the most common types.

The design of this array-level intermediate representation is intentionally constrained: it is expressive enough to support transformations such as fusion, but restricted enough to limit the

Table 2. A selection of node types commonly found in ADFGs.

Node type	Example(s)
<b>Data</b> Constant, numerical-valued data arrays	
<b>Placeholders</b> Yet-to-be-supplied input arrays	
<b>Index lambdas</b> Elementwise algebraic operations	
<b>Reshapes</b> Changes to logical array shape	
<b>Indexing</b> Array slicing and indirect indexing	
<b>Einsums</b> Einstein-summation-like operations	
<b>Joins</b> Concatenation, stacking, etc.	
<b>Functions</b> “Outlined” function definitions and calls	
<b>Communication</b> Distributed sends and receives	

complexity of implementing such transformations. Unlike other IRs such as LLVM IR or MLIR, MIRGE’s ADFG does not use indirection (e.g., name strings) when referring to nodes, but rather direct object references. This means that the ADFG is more expensive to modify, as it requires graph traversals for each transformation, but on the other hand it does not require maintaining a global state or name mapping. Together with the immutability of the array node data structure, this design choice simplifies the notion of equality between graphs and makes it easier to find redundant computation.

**4.1.1 Compilation and Freezing.** As operating on lazy arrays simply appends nodes to the ADFG, intervention is required to trigger code generation and execution. Early approaches to this issue (e.g., [40]) tended to trigger code generation implicitly, such as when array entries were retrieved by the user. Unfortunately, doing so incurs high and repeated costs rooted in building and processing of ADFGs, at least to a point where existing code can be retrieved from cache. In MIRGE, we thus pursue a more explicit approach, with two interfaces available to the user: If the code is intended to be called once, the user evaluates their array code and passes it to `actx.freeze()` to trigger the rest of the pipeline, generate and ultimately execute the code. If the code is intended to be executed multiple times, the user instead passes a function to `actx.compile()`, which evaluates it using placeholder inputs, triggers the rest of the pipeline, and returns an object that can be used for repeated execution. Examples of both of these are shown in Figure 5.

It is important to note that the implementation of `compile()` itself is also lazy. At the time of calling `compile()`, arguments that will be passed to the compiled function are unknown; in order to avoid burdening the user with the specification of argument metadata up front, `compile()`

```

a = actx.from_numpy(np.random.rand(5,2))

a_sum_sq = actx.numpy.sum(a**2) # ADFG
a_sum_sq_frozen = actx.freeze(a_sum_sq) # device array
a_sum_sq_np = actx.to_numpy(a_sum_sq_frozen) # numpy array

```

(a) Using freeze().

```

def sum_sq(x):
    return actx.numpy.sum(x**2)

sum_sq_compiled = actx.compile(sum_sq)

a = actx.from_numpy(np.random.rand(5,2))

a_sum_sq = sum_sq_compiled(a) # device array
a_sum_sq_np = actx.to_numpy(a_sum_sq) # numpy array

```

(b) Using compile().

Fig. 5. Methods for triggering code generation/execution when using lazily-evaluated arrays.

defers most of its processing until the first time the compiled function is called. This also allows the same compiled function to be called with different configurations of optional arguments; separate code will be generated for each case, with reuse occurring when applicable.

**4.1.2 Distributed Computation.** In MIRGE, array-context-based calculations may be distributed across multiple compute units. Therefore, consideration must be given to the representation of ADFGs that result from lazy evaluation in such environments. One approach, analogous to a *single control* stream model of computation (PGAS, distributed arrays), is to construct a shared, global ADFG containing the entire calculation. A naïve implementation of this, while workable at small scales, breaks down when constant array data (such as connectivity data in a finite element mesh) becomes too large to fit in a single compute unit’s memory. More sophisticated variations may be able to avoid such problems by storing constant data separately from nodes, but this increases the amount of bookkeeping required when applying transformations to the ADFG. Instead, we take the approach of *multiple control streams*, constructing separate, local ADFGs for each compute unit and embedding nodal representations of inter-process communication within them. From the perspective of a user, this amounts to writing the application much like a typical MPI-based code, but rather than calling out to MPI directly, special routines are called to create send and receive nodes and to insert them into the ADFG.

One challenge to this approach is that sends are not arrays in a dataflow sense; they are “dead end” nodes without an output. This makes them unsuitable for direct representation in an ADFG. Presently, the MIRGE infrastructure circumvents this issue by introducing a node type that: (1) acts as a passthrough for an existing array in the ADFG, and (2) holds a reference to the data (as represented by an ADFG node) to be sent. While this approach is viable, it is not without downsides. Namely, one must ensure that the sub-expression containing the send is retained as a dependency of the ADFG (in other words, its result is used in the overall computation); otherwise, unpaired communication (i.e., a receive without a send or vice versa) may result. Alternative methods, such as explicit tracking of sends in user APIs, are under investigation.

**4.1.3 ADFG Functions.** Because the dataflow graphs are generated through symbolic execution of array code, function calls are not automatically represented explicitly. Instead, each function call creates a new subgraph of its operations, analogous to inlining the code for each call. As a result, the ADFG size can grow, leading to increased processing time. Hence, it is beneficial to provide a means of selectively “outlining” functions — i.e., preventing a function call from being inlined into the ADFG.

When a function is outlined, instead of directly returning the inlined nodes for the operations of a function, a node representing the function call is returned. This node contains a representation of the function’s nodes that is isolated from the rest of the ADFG by using placeholders for the

function arguments. The corresponding concrete arguments are also stored separately in the call node. An example is shown in Figure 6.

Representing function calls explicitly in the ADFG allows them to be processed by the downstream code generation pipeline into kernel functions, or in certain cases to be optimized via ADFG transformation. See Section 4.2.4 for an example of this.

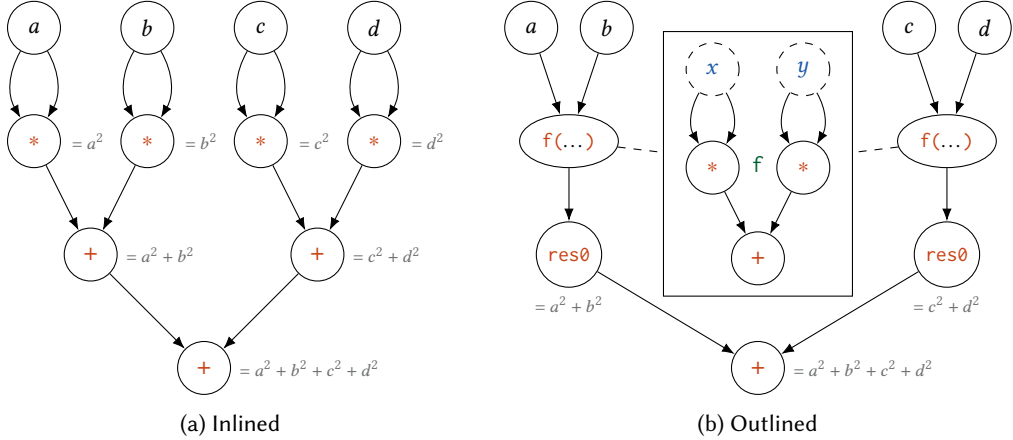


Fig. 6. An example of function outlining for an ADFG containing two calls to a function  $f$  that computes the sum of the squares of inputs  $x$  and  $y$ . Note: functions can have multiple results, hence call nodes ( $f(\dots)$ ) and result nodes ( $res0$ ) are represented separately in the ADFG.

## 4.2 Stage 2: Transform the Array DFG

With an initial dataflow graph in place, the graph is parsed and transformed to prepare for the later stages. This includes identifying mathematical simplifications in the graph, marking nodes for storage (or *materialization*), organizing the graph for distributed execution, and concatenating certain function calls for efficiency. We detail each of these concepts next; as a whole they represent the “transformation stage” of the ADFG.

**4.2.1 Apply Math Simplifications.** Transformation tools in MIRGE are used to apply mathematical simplifications to the intermediate ADFG. One example is *constant folding*, where pieces of the computation that depend only on constant data are evaluated ahead-of-time, as illustrated in Figure 7.

**4.2.2 Materialization.** The ADFG created by the computation does not initially contain any notion of *materialization*, that is, which arrays in the graph are to be stored explicitly in memory. It is therefore the responsibility of the transformation chain to make this decision. For the sake of arithmetic intensity, the fraction of arrays in the graph that are materialized should remain small. On the other hand, under-materializing can lead to excessive repeated work, as unmaterialized arrays are evaluated every time they are referenced (see Figure 8 for some examples). Thus the materialization algorithm requires a balance between these two extremes.

We currently use a greedy materialization strategy based on a simple heuristic: materialize nodes that have *more than one materialized predecessor and more than one successor*. In addition, all nodes containing reductions (in our case, typically einsum nodes) are forcibly materialized due to their increased arithmetic intensity.

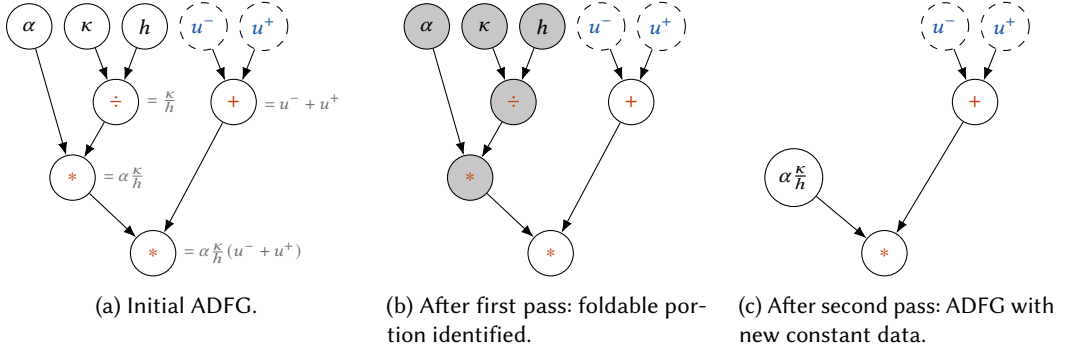
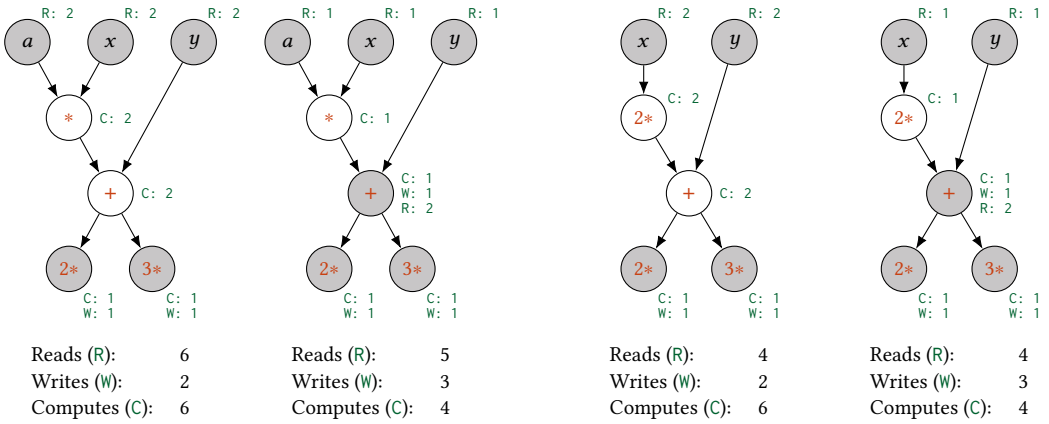


Fig. 7. Constant folding for an expression that operates on a mixture of constant data ( $\alpha$ ,  $\kappa$ , and  $h$ ) and placeholders ( $u^-$ ,  $u^+$ ).

For a number of physical models, we have found this simple approach to work well: it is both straightforward to apply and delivers acceptable results (limiting materialization rates to 5-15% and repeated computation to less than 10%). Applying this strategy to several of our more complex physical models, however, did reveal some shortcomings: (1) smaller-sized arrays whose entries are used repeatedly in the evaluation of a single larger array leading to unnecessary recomputation due to the larger array being counted as a single successor, and (2) simple sub-expressions (fewer than two materialized predecessors) that have a large number of successors. In at least one of the ADFGs we have considered, the missed materializations led to recomputation rates of over 75%. Despite this, extending the heuristic to naively materialize in these cases did not prove fruitful: computation times remained the same or increased slightly. Given that our applications are largely memory-bandwidth-bound, it is likely that the reduction in floating point operations from materializing in such cases is counteracted by an increase in memory accesses. An example of how this can happen is shown in Figure 8b. We expect that future research on improved heuristics, particularly ones that more tightly integrate with transformations applied later in the pipeline, has the potential to lead to drastic improvements.

**4.2.3 Distributed Partitioning.** To facilitate distributed-memory computation, ADFGs containing communication nodes are analyzed to determine a coarse-grained communication graph in which each node represents a communication operation (both a send and a receive), and each edge represents rank-local data flow. Individual segments are computed on each compute unit and then sent to a coordinating compute unit for processing. This coordinator computes a topological ordering of communication operations and greedily groups them into batches (Figure 9a). After the communication batches are formed, they are distributed back out to all compute units, where they are subsequently treated as boundaries between the to-be-constructed node-local computational sub-ADFGs. Computational nodes from the full ADFG are inserted between batches: (1) after all of their prerequisite receives have been completed, and (2) just before their outputs are needed (Figure 9b).

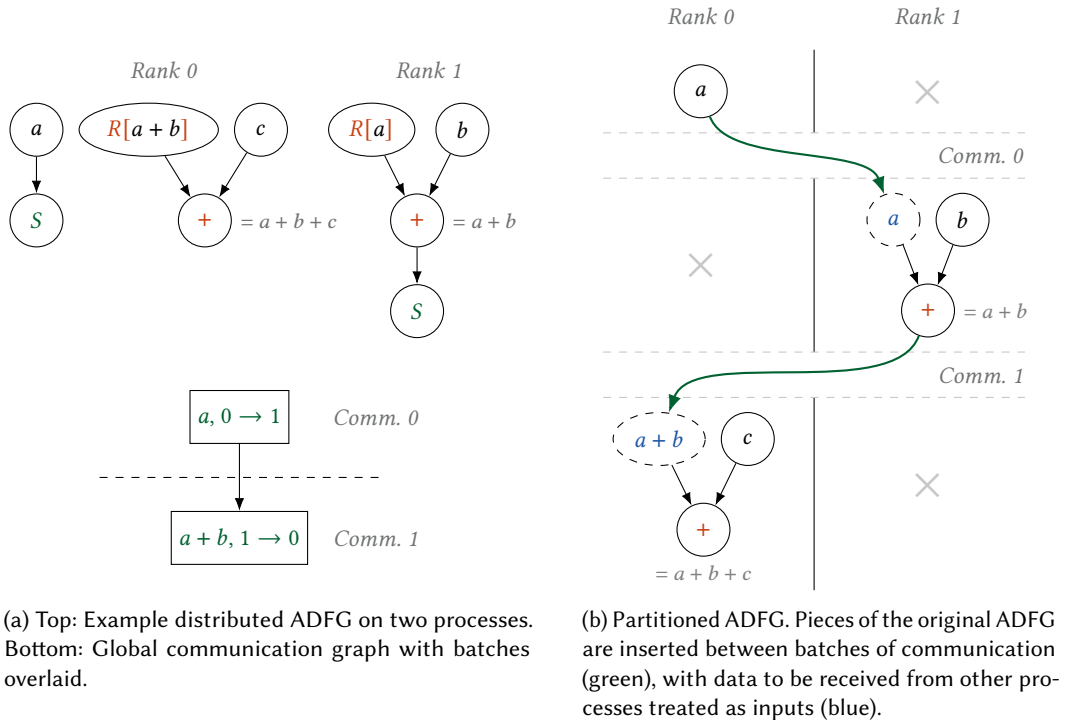
Constructing the communication graph globally guarantees that the partitioning process will not result in any circular dependencies between node-local per-batch compute-only ADFGs. A further benefit of the global communication graph is that it enables analyses to check for mismatched communication. While this solution is certainly not asymptotically scalable, in practice, we have not found this choice to result in any significant runtime burden at problem scales of relevance.



(a) A successful materialization choice (of  $ax + y$ ) that reduces computation without increasing memory accesses.

(b) A less successful materialization choice (of  $2x + y$ ) that reduces the amount of computation but increases the number of memory accesses.

Fig. 8. Two examples of materialization, showing their costs before and after in terms of array reads (R), writes (W), and computes (C). Unmaterialized nodes are shown in white; materialized nodes are shown in gray.



(a) Top: Example distributed ADFG on two processes. Bottom: Global communication graph with batches overlaid.

(b) Partitioned ADFG. Pieces of the original ADFG are inserted between batches of communication (green), with data to be received from other processes treated as inputs (blue).

Fig. 9. Partitioning a distributed ADFG. Note: For this two-rank example, destination ranks of sends (S) and source ranks of receives ( $R[\dots]$ ) are trivial and thus omitted.

**4.2.4 Concatenation of Function Calls.** If the operations inside an outlined function (see Section 4.1.3) are sufficiently ‘well-behaved’ (see below), it is possible to transform a collection of independent calls into a single call by concatenating the inputs, outputs, and function body nodes of each call along suitable axes to create a single, larger function call (as shown in Figure 10). This transformation lowers computational cost by reducing the number of kernel invocations and increasing the size of the arrays being operated on, improving GPU utilization.

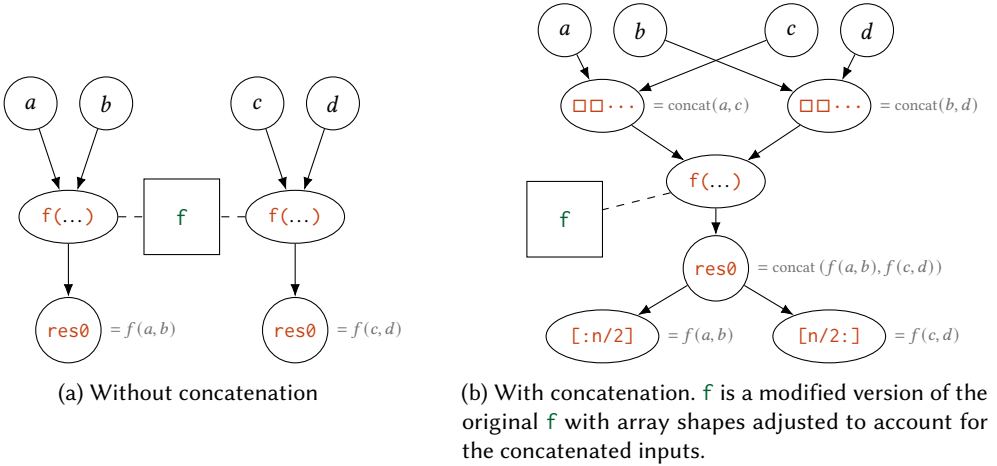


Fig. 10. Transforming an ADFG by concatenation of function calls. For simplicity, this example assumes  $a$ ,  $b$ ,  $c$ , and  $d$  are one-dimensional arrays of equal length  $n$ .

The definition of ‘well-behaved’ depends on a number of specifics. At the outset, all calls to specific user-identified functions are considered eligible for concatenation. Concatenation groups are then split to ensure that all concatenated invocations are independent. Finally, an axis matching procedure determines axes along which concatenation can take place while leaving the remaining array dimensions unchanged. We have explored a number of different algorithms for this matching, varying by their tolerance to varying axis positions. Ultimately, a relatively simple algorithm based on connecting axes at the input of a node to those at the output proved sufficient.

### 4.3 Stage 3: From Array-Level IR to Scalar IR

After the ADFG has been transformed and optimized, the next stage rewrites the graph into a lower level intermediate representation, typically expressed in the *Loopy* programming model (see [37] for details). This stage introduces loop structures, temporaries, and control flow, and makes execution order and memory usage explicit for the first time. While the ADFG deals with whole-array expressions and symbolic graphs, the *Loopy* model operates on a scalar, polyhedral model of computation, where computations are indexed over loop domains, memory layout is defined precisely, and execution order can be controlled via dependencies and tags – see Figure 11 for an example. This lowering stage operates by converting each node to *array comprehension* form, in which a formula for each array entry is given in terms of entries of its materialized predecessors. Once these array comprehensions are available, they are straightforwardly turned into assignment statements, each wrapped in a separate loop nest.

```

kn1 = lp.make_kernel(
    "{ [i,j,k]: 0 <= i < 3 and 0 <= j < 3 and 0 <= k < n_dot }",
    """
    dot = sum(k, w[k] * x[k])
    result[i * 3 + j] = x[idx[i,j]] + dot
    """
)

```

Fig. 11. An example *Loopy* kernel.

#### 4.4 Stage 4: Scalar IR Transformations

With the low-level IR in place, additional transformations are applied to target parallelization opportunities and optimizations in the memory hierarchy. In particular, *loop fusion* is critical to reduce the potentially large number of separate loops generated in the preceding stage.

In order to perform loop fusion, we rely on descriptive metadata that is (sparsely) attached to array axes in the ADFG. In our case, axis metadata is attached within the discontinuous finite element infrastructure, not within the application-level code. The main purpose of this metadata is to identify types of array axes, for example, whether an axis is indexed by the element number of a certain discretization, the physical dimension, or the degree of freedom inside an element of a certain local element type. This metadata is then propagated to all ‘connected’ axes in the ADFG and survives into the scalar IR as metadata attached to loops.

Loops with matching metadata become *fusion candidates*. Across each set of candidates, a greedy loop fusion algorithm from the literature [35], with minor modifications, selects a suitable set, while considering the nature of the dependencies among loop nests.

Next, we perform *array contraction*. As an example, consider the loop nest in Figure 12. Since the outbound dependencies surrounding the variable `tmp` are elementwise, only a single entry of the array is needed within each trip through the loop, allowing the array reference `tmp[i]` to be replaced with a scalar temporary `tmp`. We again follow a simple approach from the literature [42] to realize this transformation.

It is useful to recognize that this step will effectively undo some of the materialization decisions made earlier in the pipeline (cf. Section 4.2.2), once the profitability of the corresponding opportunities has become apparent through, chiefly, loop fusion. In future work, we hope to pursue a more integrated approach that will very likely help to reduce transform cost.

```

tmp = [None] * n
z = [None] * n
for i in range(n):
    tmp[i] = x[i] + y[i]
    z[i] = 2*tmp[i]

```

(a) Before contraction.

```

z = [None] * n
for i in range(n):
    tmp = x[i] + y[i]
    z[i] = 2*tmp

```

(b) After contraction.

Fig. 12. An illustration of array contraction using Python pseudocode. Contraction replaces the intermediate array `tmp` with a scalar temporary, reducing memory usage.

A final use of the propagated array axis/loop variable metadata allows us to identify candidates for parallelization, mostly via mapping to the hardware-parallel axes available in the GPU programming model.

#### 4.5 Stage 5: Emit Target Code / OpenCL

After the transformations described in the previous section, the code in the scalar IR has arrived at the same level of abstraction as conventional OpenCL/CUDA code. In our case, OpenCL code is generated and just-in-time compiled via various vendor implementations, particularly *PoCL* [34] and the RoCM AMD GPU OpenCL ICD. Figure 3 shows an example of the type of code generated in a simple setting.

This generation is mostly straightforward, although a number of aspects account for about 25% in Figure 4. Contributing factors include: (1) The amount of code generated. A typical workload as described in the subsequent section will emit about 100 GPU kernels, across about 10,000 lines of code. (2) It is worth noting that *loopy*'s IR is itself unordered, necessitating an ordering pass with associated validity checking. (This appears in the figure as 'linearization'.) (3) Since *loopy* is based on the polyhedral model, many operations involve core polyhedral primitives. While fairly low-cost individually, their sheer number accounts for considerable cost.

For NVIDIA devices, we typically eschew NVIDIA's vendor implementation of OpenCL, preferring *PoCL*'s CUDA target. This helps us avoid various observed performance limitations as well as the notable absence of a profiling capability on the vendor implementation. *PoCL*'s NVIDIA target makes use of LLVM's NVPTX backend, which generates NVIDIA's proprietary PTX intermediate language. The latter is then just-in-time compiled into a device binary for use on the hardware via the GPU driver. To help the viability of this approach, we have contributed a number of developments to *PoCL*'s NVIDIA target [52], notably around the use of 32-bit pointer arithmetic for scratchpad/shared memory, the use of unified/virtual memory, as well as the resolution of a pointer aliasing issue relating to scratchpad/shared memory.

#### 4.6 Stage 6: Execute

Final code execution in the case of a single compute unit is straightforward and occurs by enqueueing OpenCL kernel invocations from optimized, generated Python code (an 'invoker' in *loopy*). Our use of OpenCL allowed the use of a large range of compute hardware through a unified runtime, though with a wide array of actual vendor implementations, including *PoCL* (CPU and NVIDIA GPU), AMD ROCm, NVIDIA CL, Intel CL, and Apple CL.

**4.6.1 Distributed Execution.** To execute a partitioned computation graph, the execution engine first posts non-blocking (MPI) receive operations for all expected incoming data across all communication batches. Then, it proceeds through an event-driven loop in which any ADFG part local to the compute unit is eagerly executed as soon as its dependencies (local and remote) are satisfied. Once the GPU completes computation on the ADFG part, in turn, any necessary send operations are posted, again in a non-blocking, MPI-based fashion. This process continues until execution of all ADFG parts is complete. Resource management is handled through reference counting of arrays, automatically reclaiming memory when arrays are no longer needed by any remaining parts.

Opportunities remain for additional efficiencies, namely in overlapping computation and communication. For example, sends are not performed as soon as the data is ready, only after the current part ends. Likewise, some careful attention to scheduling could likely eliminate some measure of GPU idle time.

**4.6.2 Kernel Profiling Support.** Kernel profiling in MIRGE is enabled through the built-in event profiling capabilities in OpenCL, including functionality to track and measure the execution time of kernels during computation using specialized profiling array contexts. Profiling is managed by storing OpenCL events related to the start and stop times of kernel executions. At present, this

accounting is performed at the granularity of a GPU kernel launch. Further research is needed in order to aid the user in mapping cost to individual segments of the ADFG.

## 5 Applications

The MIRGE approach is internally complex, but this is balanced with an outward focus on productivity: our intent is to deliver optimized multiphysics simulations on a range of architectures without burdening application developers with hardware idiosyncrasies. In this section we provide numerical examples that highlight the use of MIRGE in practice. We demonstrate it through *MIRGE-Com* [6], the simulation library for the Center for Exascale-enabled Scramjet Design (CEESD) [18] at the University of Illinois Urbana–Champaign. *MIRGE-Com* is a portable, massively parallel DG library capable of simulating reactive mixture viscous flows and coupled material responses, with a main objective of predicting the internal behavior of scramjet combustors.

We consider three main cases:

- (1) an isentropic vortex in an inviscid flow,
- (2) flows exhibiting shock and boundary-layers, and
- (3) a large-scale scramjet simulation.

### 5.1 *MIRGE-Com*

The stack of packages that implements the stages of the previous sections in *MIRGE-Com* includes *pytato*<sup>2</sup> and *arraycontext*<sup>3</sup>, which facilitate the description of the code as an ADFG, and *loopy*<sup>4</sup>, which provides the IR and transformation tools. The mesh description and DG components are implemented with the help of *meshmode*<sup>5</sup>, *modepy*<sup>6</sup>, and *grudge*<sup>7</sup>.

For distributions across multiple processing elements, *MIRGE-Com* uses host-based MPI through *mpi4py* Python bindings. Portability is achieved with a lightweight installation utility, *emirge* [19] which installs a Conda environment containing components that implement MIRGE, along with the *MIRGE-Com* interface. The resulting environment supports out-of-the-box execution on most systems; more details can be found at <https://github.com/illinois-ceesd/mirgecom>.

### 5.2 *MIRGE-Com* vs. *MFEM*

In these experiments, we compare the runtime performance of *MIRGE-Com* to that of the open-source finite-element library *MFEM* [7]. We present timing data for both codes, yet it is important to recognize that strictly maximizing performance is not the only goal. This is only a general point of comparison since the two applications differ significantly in their design, implementation, user experience, and portability. *MFEM* is a C++ library with tuned optimizations for both CPU and GPU platforms. It is a reference for broadly assessing the efficiency of *MIRGE-Com* relative to an established package. Analysis of the performance of the transformed code at the core of MIRGE is reported elsewhere (for example, see [37]).

We first assess the baseline CPU performance of *MIRGE-Com* on a canonical flow benchmark case: an isentropic vortex in an inviscid flow on a periodic domain. This flow application is a packaged *MFEM* example. In both implementations, the Euler equations for compressible inviscid flow are solved using a DG discretization using tensor product elements (TPEs), and advanced in

<sup>2</sup><https://github.com/inducer/pytato>

<sup>3</sup><https://github.com/inducer/arraycontext>

<sup>4</sup><https://github.com/inducer/loopy>

<sup>5</sup><https://github.com/inducer/meshmode>

<sup>6</sup><https://github.com/inducer/modepy>

<sup>7</sup><https://github.com/inducer/grudge>

time with explicit 4th-order Runge–Kutta. GPU execution is not supported directly in *MFEM*'s inviscid vortex example, so this comparison is presented on an Apple M2 processor.

We note that it is also straightforward to run *MIRGE-Com* on GPUs, which is a more attractive target platform for modern applications. To demonstrate GPU execution, we compare the runtime performance of *MIRGE-Com* to that of *MFEM* for the scalar advection equation in a periodic domain. GPU execution is supported in *MFEM* for this example application through the use of a partial assembly of the DG operators, greatly reducing the memory footprint at the cost of added computation. *MIRGE-Com*, on the other hand, does full assembly of all DG operators, at the expense of increased memory footprint and traffic. The time per time-step for both *MIRGE-Com* and *MFEM* are shown in Figure 13 for both CPU and GPU execution. For smaller numbers of elements, *MIRGE* has a clear performance floor, which is associated with the cost of the OpenCL kernel dispatch layer in *MIRGE-Com*, which is used on both CPU and GPU platforms. A GPU performance floor is also apparent in the *MFEM* GPU execution time. *MFEM* uses AMD's Heterogeneous-computing Interface for Portability (HIP) API [5] to implement GPU-ready kernels, which are statically compiled.

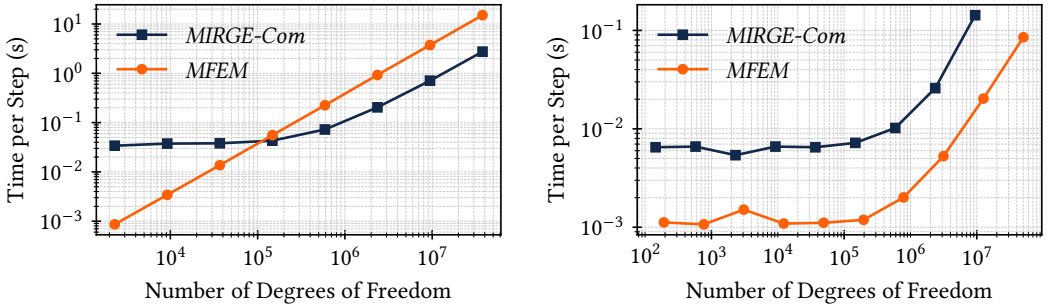


Fig. 13. Mesh scaling ( $h$ -refinement) for *MFEM* and *MIRGE-Com*. Left: inviscid vortex on an Apple M2 processor for  $p = 4$  TPEs, and fixed step 4th-order Runge–Kutta (RK4). Right: scalar advection equation using  $p = 1$  TPEs on an AMD MI300A.

### 5.3 Shock Cases vs. *Ryujin*

We next consider cases with shocks, where overintegration, artificial viscosity, and shock limiting are needed to stabilize the flow. These more complex flows and discretizations lead to correspondingly complex ADFGs to process, which help test the robustness of the *MIRGE* approach.

As a reference point, we implement experiments in both *MIRGE-Com* and in the *Ryujin* package [45, 29], which is an application of *deal.ii* [9] for compressible flow.

The first example is the classic setup of an inviscid flow past a forward-facing step, with a domain as shown in Figure 14. A perfect gas is assumed ( $\gamma = 1.4$ ), and adiabatic slip conditions are imposed on the top and bottom portions of the boundary. At the inflow,  $\Gamma_{\text{in}}$ , a Mach  $M = 3$  inflow speed is set, while no boundary conditions are imposed at the supersonic outflow  $\Gamma_{\text{out}}$ . With velocities non-dimensionalized by speed of sound, the flow is initialized with velocity  $(u, v) = (3, 0)$ .

The mesh has  $\sim 1.6\text{M}$  and  $\sim 1\text{M}$  degree-1 TPEs for *MIRGE-Com* and *Ryujin*, respectively (totaling  $\sim 6.6\text{M}$  and  $\sim 4.1\text{M}$  DOFs for each scalar quantity). A bow shock quickly forms due to the step and grows to reflect from the top boundary, creating a Mach stem and set of reflected shocks.

Figure 14 shows the magnitude of the density gradient, scaled by the maximum value, at a simulation time after the Mach stem has formed. Both *MIRGE-Com* and *Ryujin* show the strong bow shock ahead of the step, as well as a Mach stem caused by reflection from the top boundary.

Shock reflections from the triple point and top/bottom walls are also visible. Slight differences can be observed in the vortices shed from the triple point, the intersection of the bow shock and Mach stem. There is a close agreement in the resulting flows produced by *MIRGE-Com* and *Ryujin*, and the differences are attributed to differences in the underlying discretizations, e.g. continuous Galerkin (CG) in the case of *Ryujin*, a different limiter, and the use of artificial viscosity. Moreover, *Ryujin* solves the compressible Euler equations, while *MIRGE-Com* solves the full compressible Navier-Stokes equations.

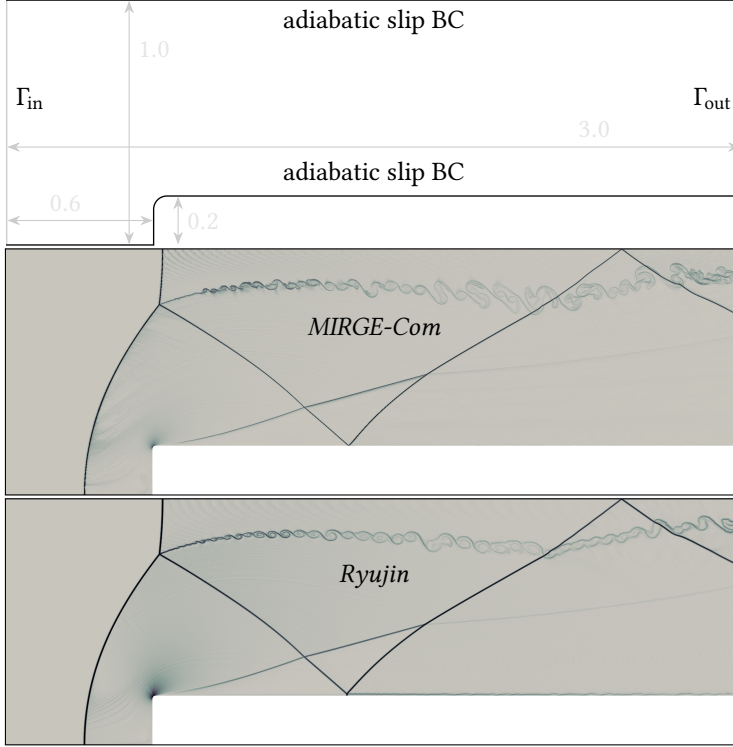


Fig. 14. Inviscid flow past a forward-facing step. Problem setup is shown at top with *MIRGE-Com* results (middle) and *Ryujin* results (bottom) are shown for magnitude of the density gradient at an advanced simulation time.

Next, we consider the interaction of a shock wave with a boundary layer. The domain is described in Figure 15, and a perfect gas is assumed ( $\gamma = 1.4$ ). The fluid is initialized at rest,  $(u, v) = (0, 0)$ , with a discontinuity in the density, with  $\rho_L = 120.0$  in  $\Omega_L$  and  $\rho_R = 1.2$  in  $\Omega_R$ , and with pressure prescribed by the isentropic flow relations:  $P = \rho/\gamma$ . Adiabatic slip conditions are imposed on the top and sides, while an adiabatic no-slip condition is imposed on the bottom of the domain. These conditions generate a shock wave that travels from left to right towards a reflective wall. A boundary layer forms along the bottom wall as the shock traverses over it. Upon reflection from the end wall, the shock interacts with the boundary layer, depositing vorticity due to the misalignment of the density and pressure gradients.

The *MIRGE-Com* mesh has 2M TPEs with degree-1 bases (8M DOFs), while the *Ryujin* mesh has  $\sim 2.1$ M elements (8.4M DOFs). Figure 15 shows the magnitude of the density gradient, scaled by the maximum value, at a simulation time after the fluid has developed.

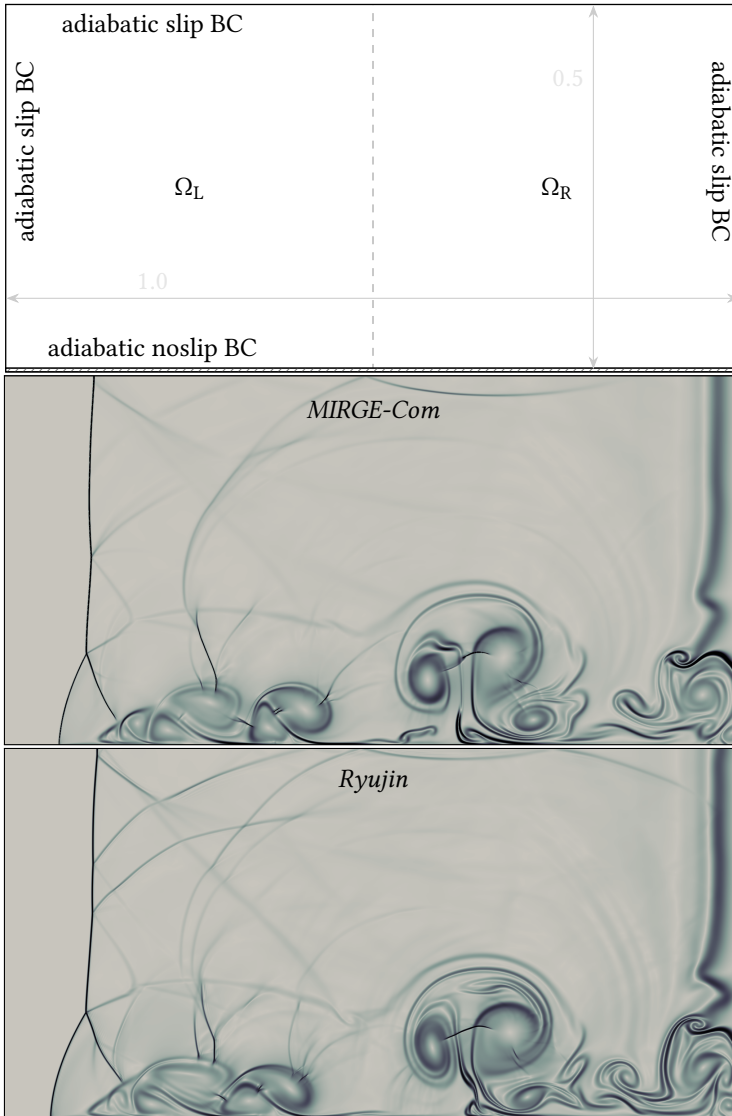


Fig. 15. Shock wave interaction with a boundary layer. Problem setup is shown at top with *MIRGE-Com* results (middle) and *Ryujin* results (bottom) are shown for magnitude of the density gradient at an advanced simulation time, after shock reflection.

The use of different models and discretizations, makes a direct comparison of performance difficult. Nevertheless, the raw numbers are informative and we report the right-hand-side (RHS) evaluation times for both applications on an Apple M2: the throughput for *Ryujin* is approximately 3.8M DOFs per second, while the throughput for *MIRGE-Com* is approximately 1.6M DOFs per second. *MIRGE-Com* also benefits substantially from its portability and device-readiness. Exercising this benchmark on an AMD MI300A device, for example, *MIRGE-Com* RHS throughput was 100.4M DOFs per second.

A natural counterpart to performance is productivity, and one beneficial feature of *MIRGE-Com* is that extending and modifying the model is relatively straightforward, due to its array-centric design and the expressiveness of Python. To quantify productivity, one metric is total lines of code, for example  $\sim 48.4\text{k}$  lines in the case of *Ryujin* (without *deal.ii*) and  $\sim 21.1\text{k}$  in *MIRGE-Com* (without subpackages such as *pytato*). In the end, however, lines of code does not fully capture the ease of adding new features (in Python) and the value of device-ready portability.

#### 5.4 Complex Geometry Simulation

*MIRGE-Com* is used by CEESD in a real-world science application to predict the behavior of a lab-scale scramjet combustor experiment conducted in the Arc Heated Combustion Tunnel-II (ACTII) facility [27, 55] at Illinois. The ACTII experimental apparatus and its computational counterpart are shown in Figure 16. In this simulation, the mesh of 34M TPEs resulted in over 3B DOFs for a three-dimensional gas-domain simulation. The computation and mesh are distributed among processing elements using Metis [47].

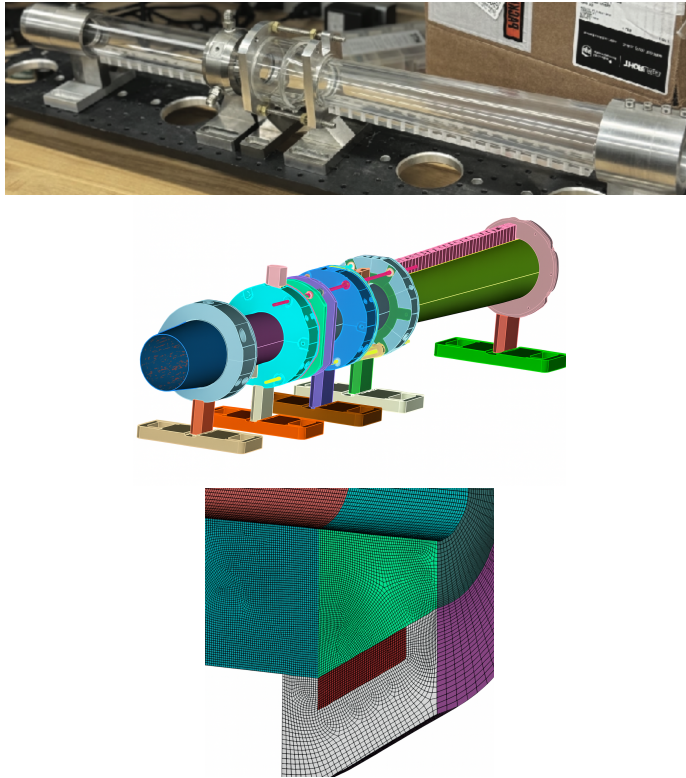


Fig. 16. (top) ACTII supersonic combustion apparatus [image credit: Izzi Gessman, Illinois] (middle) raw CAD model [CAD Credits: Qili Liu, Izzi Gessman, Mike Anderson, Illinois]; and (bottom) a section of the computational mesh produced using Coreform [22].

The simulation was conducted using (based on convenience and availability) a variety of computational platforms, while many scoping simulations and capability developments were conducted on laptops (both Intel/Linux and Apple). The development and scoping runs support large-scale simulations which run on HPC resources at DOE National Laboratories, particularly the LLNL

Tuolumne system, which is equipped with AMD MI300A accelerators. A snapshot of the capstone simulation is shown in Figure 17.

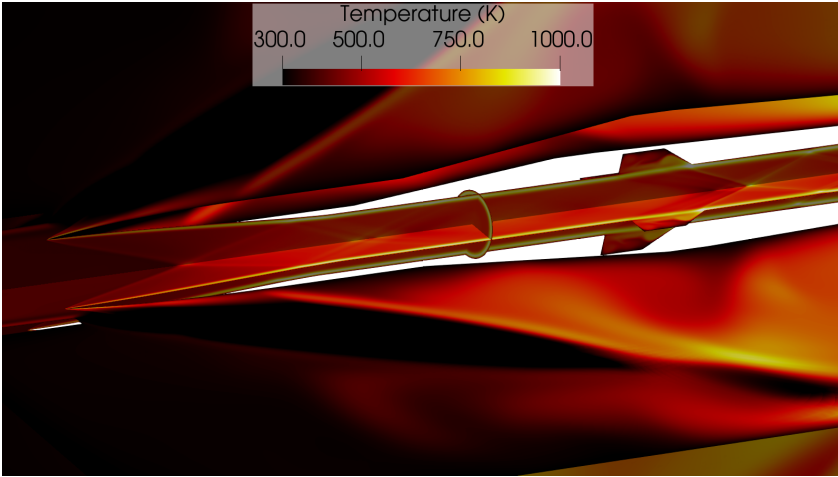


Fig. 17. Section of the scramjet combustor simulation using 256 AMD MI300A APUs on the Tuolumne platform at LLNL.

The parallel scalability of the simulation is important as the trend can be used to estimate both the computational resource required and the expected time-to-solution (TTS) for a given simulation. Here, we assess the performance of the large-scale scramjet simulation on the Tuolumne platform at LLNL, measuring both *weak* and *strong* parallel scalability.

**Weak scaling** measures the performance of a larger problem given a larger computational resource. Figure 18 shows weak scaling results for a 1D gas shock impacting a gas-material interface in a three-dimensional domain, which offers a baseline for the full scramjet simulation. The weak scaling results demonstrate that *MIRGE-Com* can achieve near-ideal scaling to full machine scale for this leadership-class HPC platform.

**Strong scaling** measures the performance of fixed-size problem faster given a larger computational resource. For this test we fix the mesh size in the simulation at  $\sim 3\text{M}$  elements (or  $\sim 1.26\text{B}$  DOFs), resulting in  $\sim 80\text{M}$  DOFs per rank to  $\sim 2.5\text{M}$  DOFs per rank as we scale the number of GPUs from 16 to 512. Figure 19 shows strong scaling, where we observe good scaling out to 256 ranks for this run, which was more than sufficient for conducting the desired simulations with reasonable turn-around time.

The MIRGE process often obscures the code-to-kernel connection, making it a challenge to correlate the resulting kernels with expected performance of specific DG operations. The MIRGE infrastructure transforms the application code dynamically at runtime, and the transformations are problem and configuration specific. Our expectation for low-order ( $p \leq 2$ ) DG is that the work is dominated by vector (BLAS-1) and matrix-vector (BLAS-2) [17] operations, yielding kernels with low arithmetic intensities and a memory bound execution.

To evaluate the absolute performance of *MIRGE-Com*, we examine the roofline performance [59] for the most expensive kernels (i.e. those in which the application spends the most time) generated by the MIRGE process for the scramjet simulation running  $p = 1$  simplicial elements. Figure 20 presents an empirical roofline model constructed from the ten most expensive kernels, using the AMD roofline tool *rocprof-compute*; the tool empirically evaluates the arithmetic intensity and

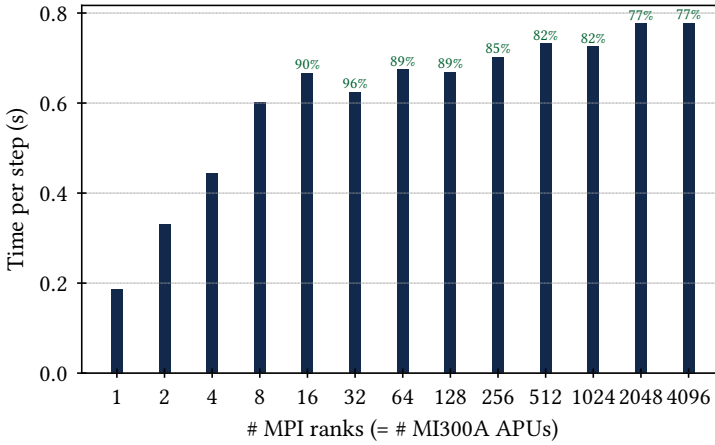


Fig. 18. Weak parallel scaling on Tuolumne (AMD MI300A) for the scramjet baseline simulation. The weak scaling parallel efficiency for  $n$  ranks versus 8 ranks ( $100 \cdot t_8 / t_n$ ) is given as a percentage.

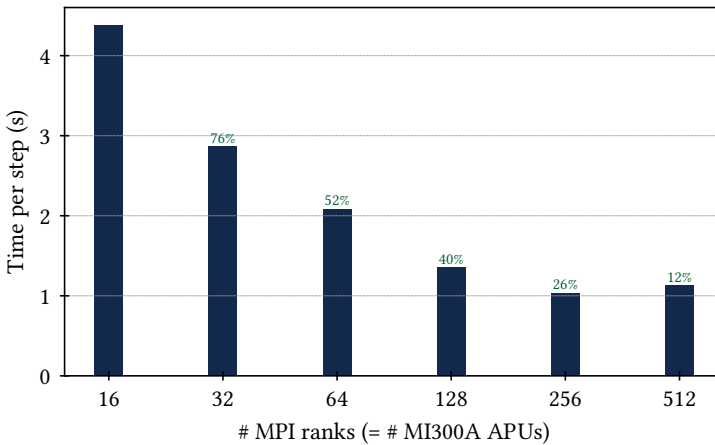


Fig. 19. Parallel strong scaling on Tuolumne (AMD MI300A) for the scramjet simulation. The strong scaling parallel efficiency for  $n$  ranks versus 16 ranks ( $100 \cdot 16 \cdot t_{16} / (n \cdot t_n)$ ) is given as a percentage.

measures the running bandwidth for the device at runtime. The roofline plot illustrates that the kernels generated for this problem run close to the expected bandwidth for main high-bandwidth memory (HBM). Kernels exceeding the HBM performance have a higher amount of data reuse (e.g., cache-coherence), while those falling significantly short of HBM bandwidth indicate kernels that could potentially be improved.

## 6 Conclusion

The MIRGE approach for array-based high-performance computing builds on the concept of *lazy evaluation* of array-based computation. By representing computation as array dataflow graphs (ADFGs), it enables transformations and optimizations that are impractical in a purely eager execution model. These graphs are lowered to a scalar IR, where traditional compiler-style transformations

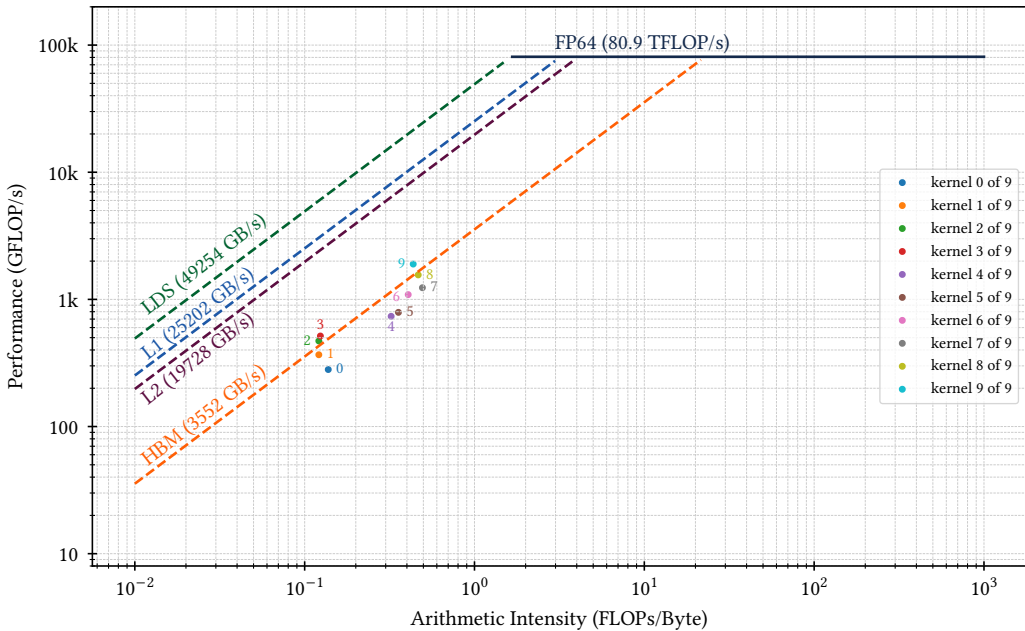


Fig. 20. Empirical roofline on Tuolumne (AMD MI300A) for top 10 most expensive *MIRGE-Com* kernels in the scramjet simulation running  $p = 1$  simplices.

such as loop fusion become possible. From there, target-specific OpenCL kernels are generated and executed. The framework also integrates distributed execution directly into the ADFG through specialized communication nodes, allowing large-scale computations to be expressed in a unified way. Demonstrations of simulations show it provides platform portability and performance loosely comparable to other finite-element flow simulation tools.

## Acknowledgments

This material is based in part upon work supported by the Department of Energy, National Nuclear Security Administration under Award Number DE-NA0003963 as well as by the National Science Foundation under Award Number 1931577.

## References

- [1] Martín Abadi. 2016. TensorFlow: learning functions at scale. In *Proceedings of the 21st ACM SIGPLAN International Conference on Functional Programming (ICFP 2016)*. Association for Computing Machinery, Nara, Japan, 1. ISBN: 9781450342193. doi:10.1145/2951913.2976746.
- [2] Ahmad Abdelfattah et al. 2021. GPU algorithms for efficient exascale discretizations. *Parallel Computing*, 108, 102841. doi:10.1016/j.parco.2021.102841.
- [3] Martin S. Alnæs, Anders Logg, Kristian B. Ølgaard, Marie E. Rognes, and Garth N. Wells. 2014. Unified form language: a domain-specific language for weak formulations of partial differential equations. *ACM Trans. Math. Softw.*, 40, 2, Article 9, (Mar. 2014), 37 pages. doi:10.1145/2566630.
- [4] Martin S. Alnæs et al. 2015. The FEniCS project version 1.5. *Archive of Numerical Software*, 3. doi:10.11588/ans.2015.100.20553.
- [5] [SW] AMD, HIP: Heterogeneous-computing Interface for Portability 2025. URL: <https://rocm.docs.amd.com/projects/HIP/en/latest/>.

- [6] [SW] Michael J. Anderson, Mike Campbell, Matthias Diener, Jonathan B. Freund, Kaushik Kulkarni, Andreas Klöckner, Luke N. Olson, and Matthew J. Smith. MIRGE-Com: Math-Intermediate Representation-Generation-Execution for Combusting high-speed flows 2025. URL: <https://github.com/illinois-ceesd/mirgecom>.
- [7] Robert Anderson et al. 2021. MFEM: A modular finite element methods library. *Computers & Mathematics with Applications*, 81, (Jan. 2021), 42–74. doi:10.1016/j.camwa.2020.06.009.
- [8] Russel Arbore, Aaron Councilman, Xavier Routh, Ryan Ziegler, Praneet Rathi, and Vikram Adve. 2025. Hercules: a compiler for productive programming of heterogeneous systems. (2025). arXiv: 2503.10855 [cs.PL]. doi:10.48550/arXiv.2503.10855.
- [9] Daniel Arndt et al. 2021. The deal.II finite element library: design, features, and insights. *Computers & Mathematics with Applications*, 81, (Jan. 2021), 407–422. doi:10.1016/j.camwa.2020.02.022.
- [10] John Backus. 1978. The history of FORTRAN I, II, and III. *SIGPLAN Not.*, 13, 8, (Aug. 1978), 165–180. doi:10.1145/960118.808380.
- [11] Satish Balay et al. 2025. PETSc/TAO Users Manual. Tech. rep. ANL-21/39 - Revision 3.24. Argonne National Laboratory. doi:10.2172/2998643.
- [12] Peter Bastian et al. 2021. The DUNE framework: basic concepts and recent developments. *Computers & Mathematics with Applications*, 81, 75–112. doi:10.1016/j.camwa.2020.06.007.
- [13] Michael Bauer and Michael Garland. 2019. Legate NumPy: accelerated and distributed array computing. In *Proceedings of the International Conference for High Performance Computing, Networking, Storage and Analysis (SC '19)* Article 23. Association for Computing Machinery, Denver, Colorado, 23 pages. ISBN: 9781450362290. doi:10.1145/3295500.3356175.
- [14] Jeff Bezanson, Alan Edelman, Stefan Karpinski, and Viral B Shah. 2017. Julia: a fresh approach to numerical computing. *SIAM Review*, 59, 1, 65–98. doi:10.1137/141000671.
- [15] [SW] James Bradbury et al., JAX: composable transformations of Python+NumPy programs version 0.3.13, 2018. URL: <http://github.com/jax-ml/jax>.
- [16] Jed Brown et al. 2021. libCEED: fast algebra for high-order element-based discretizations. *Journal of Open Source Software*, 6, 63, 2945. doi:10.21105/joss.02945.
- [17] C.L.Lawson, R.J.Hanson, D.R.Kincaid, and F.T.Krogh. 1979. Basic linear algebra subprograms for Fortran usage. 5, 308–323, 3. doi:10.1145/355841.355847.
- [18] Center for Exascale-Enabled Scramjet Design (CEESD). 2025. Center for exascale-enabled scramjet design. <https://ceesd.illinois.edu>.
- [19] [SW] Center for Exascale-Enabled Scramjet Design (CEESD), emirge: Portable installation utility for MIRGE and MIRGE-Com 2025. URL: <https://github.com/illinois-ceesd/emirge>.
- [20] Sharan Chetlur, Cliff Woolley, Philippe Vandermersch, Jonathan Cohen, John Tran, Bryan Catanzaro, and Evan Shelhamer. 2014. cuDNN: efficient primitives for deep learning. (2014). arXiv: 1410.0759 [cs.NE]. doi:10.48550/arXiv.1410.0759.
- [21] Philippe G. Ciarlet. 2002. *The Finite Element Method for Elliptic Problems. Classics in Applied Mathematics*. Vol. 40. SIAM, xxviii+530. ISBN: 0-89871-514-8. doi:10.1137/1.9780898719208.
- [22] Coreform. 2025. Coreform: simulation without compromise. <https://coreform.com>.
- [23] Adin D. Falkoff and Kenneth E. Iverson. 1978. The evolution of APL. *SIGAPL APL Quote Quad*, 9, 1, (Sept. 1978), 30–44. doi:10.1145/586040.586048.
- [24] Paul Fischer et al. 2022. NekRS, a GPU-accelerated spectral element Navier–Stokes solver. *Parallel Computing*, 114, 102982. doi:10.1016/j.parco.2022.102982.
- [25] Roy Frostig, Matthew James Johnson, and Chris Leary. 2018. Compiling machine learning programs via high-level tracing. In *Proceedings of Machine Learning and Systems*. <https://mlsys.org/Conferences/doc/2018/146.pdf>.
- [26] G. Gao, R. Olsen, V. Sarkar, and R. Thekkath. 1993. Collective loop fusion for array contraction. In *Languages and Compilers for Parallel Computing*. Utpal Banerjee, David Gelernter, Alex Nicolau, and David Padua, (Eds.) Springer Berlin Heidelberg, Berlin, Heidelberg, 281–295. ISBN: 978-3-540-48201-7. doi:10.1007/3-540-57502-2\_53.
- [27] Isabella Gessman, Shruti Ghanekar, Gyu Sub Lee, Keunsoo Kim, Nozomu Kato, Jihyung Yoo, and Tonghun Lee. 2023. Scramjet inflow characterization based on thermodynamic analysis of arc-heater plenum. In *AIAA SCITECH 2023 Forum*. (Jan. 2023). doi:10.2514/6.2023-2332.
- [28] T.R.G. Green and M. Petre. 1996. Usability analysis of visual programming environments: a ‘cognitive dimensions’ framework. *Journal of Visual Languages and Computing*, 7, 2, 131–174. doi:10.1006/jvlc.1996.0009.
- [29] Jean-Luc Guermond, Martin Kronbichler, Matthias Maier, Bojan Popov, and Ignacio Tomas. 2022. On the implementation of a robust and efficient finite element-based parallel solver for the compressible Navier–Stokes equations. *Computer Methods in Applied Mechanics and Engineering*, 389, 114250. doi:10.1016/j.cma.2021.114250.
- [30] Charles R. Harris et al. 2020. Array programming with NumPy. *Nature*, 585, 7825, (Sept. 2020), 357–362. doi:10.1038/s41586-020-2649-2.

- [31] Jan S. Hesthaven and Tim Warburton. 2007. *Nodal Discontinuous Galerkin Methods: Algorithms, Analysis, and Applications. Texts in Applied Mathematics*. Vol. 54. Springer, xiv+500. ISBN: 978-0-387-72065-4. doi:[10.1007/978-0-387-72067-8](https://doi.org/10.1007/978-0-387-72067-8).
- [32] So Hirata. 2003. Tensor Contraction Engine: Abstraction and automated parallel implementation of configuration-interaction, coupled-cluster, and many-body perturbation theories. *The Journal of Physical Chemistry A*, 107, 46, 9887–9897. doi:[10.1021/jp034596z](https://doi.org/10.1021/jp034596z).
- [33] Miklós Homolya, Lawrence Mitchell, Fabio Luporini, and David A. Ham. 2018. TSFC: A structure-preserving form compiler. *SIAM Journal on Scientific Computing*, 40, 3, C401–C428. doi:[10.1137/17M1130642](https://doi.org/10.1137/17M1130642).
- [34] Pekka Jääskeläinen, Carlos Sánchez de La Loma, Erik Schnetter, Kalle Raiskila, Jarmo Takala, and Heikki Berg. 2015. pocl: A performance-portable OpenCL implementation. *International Journal of Parallel Programming*, 43, 5, 752–785. doi:[10.1007/s10766-014-0320-y](https://doi.org/10.1007/s10766-014-0320-y).
- [35] Ken Kennedy and Kathryn S. McKinley. 1994. Maximizing loop parallelism and improving data locality via loop fusion and distribution. In *Languages and Compilers for Parallel Computing*. Utpal Banerjee, David Gelernter, Alex Nicolau, and David Padua, (Eds.) Springer Berlin Heidelberg, Berlin, Heidelberg, 301–320. ISBN: 978-3-540-48308-3. doi:[10.1007/3-540-57659-2\\_18](https://doi.org/10.1007/3-540-57659-2_18).
- [36] Robert C. Kirby and Anders Logg. 2006. A compiler for variational forms. *ACM Trans. Math. Softw.*, 32, 3, (Sept. 2006), 417–444. doi:[10.1145/1163641.1163644](https://doi.org/10.1145/1163641.1163644).
- [37] Andreas Klöckner. 2014. Loo.py: Transformation-based code generation for GPUs and CPUs. In *Proceedings of ACM SIGPLAN International Workshop on Libraries, Languages, and Compilers for Array Programming (ARRAY’14)*. Association for Computing Machinery, Edinburgh, United Kingdom, 82–87. ISBN: 9781450329378. doi:[10.1145/2627373.2627387](https://doi.org/10.1145/2627373.2627387).
- [38] Andreas Klöckner, Nicolas Pinto, Yunsup Lee, Bryan Catanzaro, Paul Ivanov, and Ahmed Fasih. 2012. PyCUDA and PyOpenCL: A scripting-based approach to GPU run-time code generation. *Parallel Computing*, 38, 3, 157–174. doi:<https://doi.org/10.1016/j.parco.2011.09.001>.
- [39] Mads R.B. Kristensen, Simon A.F. Lund, Troels Blum, and James Avery. 2016. Fusion of parallel array operations. In *Proceedings of the 2016 International Conference on Parallel Architectures and Compilation (PACT ’16)*. Association for Computing Machinery, Haifa, Israel, 71–85. ISBN: 9781450341219. doi:[10.1145/2967938.2967945](https://doi.org/10.1145/2967938.2967945).
- [40] Mads RB Kristensen, Simon AF Lund, Troels Blum, Kenneth Skovhede, and Brian Vinter. 2013. Bohrium: Unmodified NumPy code on CPU, GPU, and cluster. In *4th Workshop on Python for High Performance and Scientific Computing (PyHPC’13)*.
- [41] Kaushik Kulkarni and Andreas Klöckner. 2025. Code generation for near-roofline finite element actions on GPUs from symbolic variational forms. (2025). arXiv: [2506.17471](https://arxiv.org/abs/2506.17471) [cs.DC]. doi:[10.48550/arXiv.2506.17471](https://doi.org/10.48550/arXiv.2506.17471).
- [42] Chi-Chung Lam, P. Sadayappan, and Rephael Wenger. 1997. Optimal reordering and mapping of a class of nested-loops for parallel execution. In *Languages and Compilers for Parallel Computing*. David Sehr, Utpal Banerjee, David Gelernter, Alex Nicolau, and David Padua, (Eds.) Springer Berlin Heidelberg, Berlin, Heidelberg, 315–329. ISBN: 978-3-540-69128-0. doi:[10.1007/BFb0017261](https://doi.org/10.1007/BFb0017261).
- [43] Siu Kwan Lam, Antoine Pitrou, and Stanley Seibert. 2015. Numba: a LLVM-based Python JIT compiler. In *Proceedings of the Second Workshop on the LLVM Compiler Infrastructure in HPC (LLVM’15)* Article 7. Association for Computing Machinery, Austin, Texas, 6 pages. ISBN: 9781450340052. doi:[10.1145/2833157.2833162](https://doi.org/10.1145/2833157.2833162).
- [44] Chris Lattner et al. 2021. MLIR: Scaling compiler infrastructure for domain specific computation. In *2021 IEEE/ACM International Symposium on Code Generation and Optimization (CGO)*, 2–14. doi:[10.1109/CGO51591.2021.9370308](https://doi.org/10.1109/CGO51591.2021.9370308).
- [45] Matthias Maier and Martin Kronbichler. 2021. Efficient parallel 3D computation of the compressible Euler equations with an invariant-domain preserving second-order finite-element scheme. *ACM Trans. Parallel Comput.*, 8, 3, Article 16, (Sept. 2021), 30 pages. doi:[10.1145/3470637](https://doi.org/10.1145/3470637).
- [46] James Malcolm, Pavan Yalamanchili, Chris McClanahan, Vishwanath Venugopalakrishnan, Krunal Patel, and John Melonakos. 2012. ArrayFire: a GPU acceleration platform. In *Modeling and Simulation for Defense Systems and Applications VII*. Eric J. Kelmelis, (Ed.) Vol. 8403. International Society for Optics and Photonics. SPIE, 84030A. doi:[10.1117/12.921122](https://doi.org/10.1117/12.921122).
- [47] [SW], METIS: Serial Graph Partitioning and Fill-reducing Matrix Ordering version 5.1.0. URL: <https://github.com/KarypisLab/METIS>.
- [48] Erdal Mutlu, Ruiqin Tian, Bin Ren, Sriram Krishnamoorthy, Roberto Gioiosa, Jacques Pienaar, and Gokcen Kestor. 2022. COMET: A domain-specific compilation of high-performance computational chemistry. In *Languages and Compilers for Parallel Computing*. Barbara Chapman and José Moreira, (Eds.) Springer International Publishing, Cham, 87–103. ISBN: 978-3-030-95953-1. doi:[10.1007/978-3-030-95953-1\\_7](https://doi.org/10.1007/978-3-030-95953-1_7).
- [49] [SW], Nek5000. Argonne National Laboratory, Mathematics and Computer Science Division. URL: <https://nek5000.mcs.anl.gov>.

- [50] Ryosuke Okuta, Yuya Unno, Daisuke Nishino, Shohei Hido, and Crissman Loomis. 2017. CuPy: A NumPy-compatible library for NVIDIA GPU calculations. In *Proceedings of Workshop on Machine Learning Systems (LearningSys) in The Thirty-first Annual Conference on Neural Information Processing Systems (NIPS)*. [http://learningsys.org/nips17/assets/papers/paper\\_16.pdf](http://learningsys.org/nips17/assets/papers/paper_16.pdf).
- [51] Adam Paszke et al. 2019. PyTorch: An imperative style, high-performance deep learning library. In *Advances in Neural Information Processing Systems 32*. Curran Associates, Inc., 8024–8035. doi:10.48550/arXiv.1912.01703.
- [52] pocl. 2020. 1.6 release notes. (2020). Retrieved 2025-12-16 from <https://portablecl.org/pocl-1.6.html>. Archived at <https://web.archive.org/web/20250513114526/https://portablecl.org/pocl-1.6.html>.
- [53] Florian Rathgeber, David A. Ham, Lawrence Mitchell, Michael Lange, Fabio Luporini, Andrew T. T. Mcrae, Gheorghe-Teodor Bercea, Graham R. Markall, and Paul H. J. Kelly. 2016. Firedrake: Automating the finite element method by composing abstractions. *ACM Trans. Math. Softw.*, 43, 3, Article 24, (Dec. 2016), 27 pages. doi:10.1145/2998441.
- [54] James Reed, Zachary DeVito, Horace He, Ansley Ussery, and Jason Ansel. 2022. torch.fx: Practical program capture and transformation for deep learning in Python. In *Proceedings of Machine Learning and Systems*. D. Marculescu, Y. Chi, and C. Wu, (Eds.) Vol. 4, 638–651. [https://proceedings.mlsys.org/paper\\_files/paper/2022/file/7c98f9c7ab2df90911da23f9ce72ed6e-Paper.pdf](https://proceedings.mlsys.org/paper_files/paper/2022/file/7c98f9c7ab2df90911da23f9ce72ed6e-Paper.pdf).
- [55] Samuel Richardson, Jack R. Edwards, Isabella Gessman, Jie Lim, Arthur Paganini, and Tonghun Lee. 2025. Numerical simulation of oxygen-enhanced combustion in an arc-heated direct connect scramjet facility. In *AIAA SCITECH 2025 Forum*. (Jan. 2025). doi:10.2514/6.2025-2258.
- [56] Daniel J. Rosenkrantz, Lenore R. Mullin, and Harry B. Hunt III. 2006. On minimizing materializations of array-valued temporaries. *ACM Trans. Program. Lang. Syst.*, 28, 6, (Nov. 2006), 1145–1177. doi:10.1145/1186632.1186637.
- [57] The Theano Development Team et al. 2016. Theano: A python framework for fast computation of mathematical expressions. (2016). arXiv: 1605.02688 [cs. SC]. doi:10.48550/arXiv.1605.02688.
- [58] [SW] Vijay Thakkar et al., CUTLASS version 3.0.0, Jan. 2023. URL: <https://github.com/NVIDIA/cutlass>.
- [59] Samuel Williams, Andrew Waterman, and David Patterson. 2009. Roofline: An insightful visual performance model for multicore architectures. *Communications of the ACM*, 52, 4, 65–76. doi:10.1145/1498765.1498785.

Received X; revised X; accepted X